A&A 626, A78 (2019)
https://doi.org/10.1051/0004-6361/201935170

Astronomy & Astrophysics

Multiwavelength analysis of brightness variations of 3C 279: probing the relativistic jet structure and its evolution

Pedro P. B. Beaklini[1], Tânia P. Dominici[2], Zulema Abraham[1], and Juliana C. Motter[3]

[1] Instituto de Astronomia, Geofísica e Ciências Atmosféricas, Universidade de São Paulo, Rua do Matão 1226, 05508-090 São Paulo, SP, Brazil
e-mail: pedro.beaklini@iag.usp.br
[2] Museu de Astronomia e Ciências Afins, Ministério da Ciência, Tecnologia, Inovações e Comunicações (MAST/MCTIC), Rua General Bruce 586, 20921-030 Bairro Imperial de São Cristóvão, Rio de Janeiro, Brazil
[3] Departamento de Astronomia, Universidade Federal do Rio Grande do Sul, Avenida Bento Gonçalves 9500, 91501-970 Porto Alegre, RS, Brazil

Received 30 January 2019 / Accepted 21 April 2019

ABSTRACT

Aims. We studied the correlation between brightness and polarization variations in 3C 279 at different wavelengths, over time intervals long enough to cover the time lags due to opacity effects. We used these correlations together with VLBI images to constrain the radio and high energy source position.
Methods. We made 7 mm radio continuum and *R*-band polarimetric observations of 3C 279 between 2009 and 2014. The radio observations were performed at the Itapetinga Radio Observatory, while the polarimetric data were obtained at Pico dos Dias Observatory, both in Brazil. We compared our observations with the γ-ray *Fermi*/LAT and *R*-band SMARTS light curves.
Results. We found a good correlation between 7 mm and *R*-band light curves, with a delay of 170 ± 30 days in radio, but no correlation with the γ rays. However, a group of several γ-ray flares in April 2011 could be associated with the start of the 7 mm strong activity observed at the end of 2011.We also detected an increase in *R*-band polarization degree and rotation of the polarization angle simultaneous with these flares. Contemporaneous VLBI images at the same radio frequency show two new strong components close to the core, ejected in directions very different from that of the jet.
Conclusions. The good correlation between radio and *R*-band variability suggests that their origin is synchrotron radiation. The lack of correlation with γ-rays produced by the Inverse *Compton* process on some occasions could be due to the lack of low energy photons in the jet direction or to absorption of the high energy photons by the broad line region clouds. The variability of the polarization parameters during flares can be easily explained by the combination of the jet polarization parameters and those of newly formed jet components.

Key words. galaxies: active – galaxies: jets – quasars: individual: 3C 279 – radiation mechanisms: non-thermal

1. Introduction

One of the crucial questions in the understanding of high energy (HE) emission sources in active galactic nuclei (AGNs) is their actual location. Poor spatial resolution at this energy range is compensated by the relatively good time sampling and long-term data series provided by *Fermi*/LAT[1] since 2008 (Atwood et al. 2009). Correlations of HE emission with those at other frequencies also help in the investigation, and radio images obtained with VLBI techniques provide the best spatial resolution. The radio and millimeter-wave emission clearly originate in a compact, optically thick core and extended jet where bright components move away from the core with apparent superluminal velocities. The formation of these components has been associated with the occurrence of optical and infrared flares (Marscher & Gear 1985); correlations between optical and γ-ray events seem to put these emission regions at the same site. However, their association is not straightforward because opacity effects introduce time lags between the radio light curves and those at higher frequencies, which can compromise their interpretation and should be analyzed carefully for each source (Botti & Abraham 1988; Stevens et al. 1998; Türler et al. 1999, 2000; Chatterjee et al. 2008; Max-Moerbeck et al. 2014; Beaklini & Abraham 2014; Beaklini et al. 2017).

3C 279 is the first AGN for which superluminal motions were measured with VLBI techniques (Whitney et al. 1971; Cohen et al. 1971), and also the first to be detected as a HE emitter by the *Compton* Gamma Ray Observatory (CGRO; Hartman et al. 1992). It is one of the seven flat spectrum radio quasars (FSRQ) detected at very high energy (VHE) with the Cherenkov γ-ray observatories: High Energy Stereoscopic System (H.E.S.S.), Major Atmospheric Gamma Imaging Cherenkov Telescopes (MAGIC), and Very Energetic Radiation Imaging Telescope Array (VERITAS) (Albert et al. 2008; Marscher et al. 2010; Mirzoyan 2014, 2017; Abeysekara et al. 2015; Cerruti et al. 2017).

3C 279 presents variable emission throughout the entire electromagnetic spectrum on several timescales, showing some periods of low activity and others in which intense flares are observed (Maraschi et al. 1994; Wehrle et al. 1998; Hartman et al. 2001a; Larionov et al. 2008; Chatterjee et al. 2008; Collmar et al. 2010; Abdo et al. 2010; Aleksić et al. 2011;

[1] https://fermi.gsfc.nasa.gov/

Hayashida et al. 2012; Rani et al. 2017; Patiño-Álvarez et al. 2018). It is also a highly polarized blazar, being one of the first radio sources for which optical polarization was measured (Kinman 1967). The polarization is variable on timescales that range from hours (Andruchow et al. 2003) to several months (e.g., Abdo et al. 2010; Hayashida et al. 2012, 2015; Kiehlmann et al. 2016; Jermak et al. 2016), and the polarization degree (PD) varies from values smaller than 1% to values as high as 45%.

A historical optical light curve of 3C 279, starting in 1927, was compiled by Webb et al. (1990), who noticed a similarity in the flaring activity at two epochs separated by 50 years; Fan (1999), using 27 years of observations in the near infrared, found evidence of a 7-year periodicity in the light curve. Those periodicities, together with variations in the velocities and position angles of the superluminal jet components, were interpreted in terms of jet precession models (Abraham & Carrara 1998; Qian 2011).

3C 279 was included in the blazar sequence according to the classification scheme of Ghisellini et al. (1998), based on the HE properties of its spectral energy distribution (SED). Its two-peaked SED is a common feature in the blazar class. The first peak, between radio and X-rays, is attributed to synchrotron radiation of relativistic electrons, while the second one at γ-ray energies, is probably due to the inverse *Compton* process involving high energy electrons and low energy photons, either from the synchrotron emission (synchrotron self-*Compton*, SSC) or from an external source (external *Compton*, EC), although hadronic models are sometimes necessary to explain the VHE emission (e.g., Mannheim 1993; Böttcher et al. 2009, 2013; Liu et al. 2019). When trying to understand the SED of blazars, it is necessary to separate the contribution of their quiescent or slowly varying source from the flaring components. In 3C 279, the quiescent SED was identified from its lowest emission states (January 1993 and January 1995), which even allowed the study of the accretion disk, as reported by Pian et al. (1999).

Since the launch of the *Fermi* Space Observatory the efforts to observe the counterparts of the γ-ray emission in 3C 279 at lower frequencies have been increasing (e.g., Larionov et al. 2008; Chatterjee et al. 2008; Collmar et al. 2010; Hayashida et al. 2012; Rani et al. 2017). Multiwavelength observations have shown evidence of correlations between γ-ray and optical flares, with delays from 1 to 10 days between them (Hatman et al. 2001b; Abdo et al. 2010; Hayashida et al. 2012; Rani et al. 2017). This kind of correlation is not restricted to the optical flux density alone, but also involves variations in the optical PD and polarization angle, identified as PA (Abdo et al. 2010). However, the relation between γ-ray flares, radio and millimeter wave emission is still not clear, probably due to large time lags between the events at low and high frequencies, and the possible superposition of emission of different flares at the lower frequencies.

In this paper, we report the radio and optical polarimetric variability of 3C 279 between 2009 and 2014, with emphasis on the very intense activity at radio frequencies that started at the end of 2011 and lasted for almost a year that did not seem to be correlated with any γ-ray activity. In Sect. 2 we discuss the observational methods used in the radio observations with the Itapetinga radiotelescope and the polarimetric observations at the Pico dos Dias Observatory (OPD). In Sect. 3 we present our observational results, and in Sect. 4 our interpretation. Finally, we state our conclusions in Sect. 5.

2. Observations

The original 7 mm data presented in this work were obtained from the blazar monitoring program performed between 2009 and 2014 (MJD 55179 to MJD 56733) at the Itapetinga Radio Observatory[2] (ROI) and the *R*-band polarimetry at the Pico dos Dias Observatory[3], both in Brazil. Data at the two observatories were obtained simultaneously when possible, on a monthly basis. Previous results of this program were published by Beaklini & Abraham (2014) and Beaklini et al. (2017), corresponding to data analysis of the sources 3C 273 and PKS 1510−089, respectively. The observational methods were already described in detail in those papers and will be summarized here.

2.1. 7 mm observations at the Itapetinga Radio Observatory

The 7 mm observations were made with the 14 m radome enclosed radiotelescope, which gave a HPBW of 2.4 arc min. The on-the-fly observing method was used, in which 30 scans centered at the source were made, each with 30 arc min amplitude and 20 s duration. The scan direction was switched between azimuth and elevation to check the pointing accuracy. On a typical day between 6 and 14 observations were obtained for each scan direction. A room temperature, 1 GHz double side band *K*-band receiver was used, with noise temperature of about 700 K. A room temperature load and a noise source of known temperature were used for instrumental calibration and correction of atmospheric absorption in the presence of the radome (Abraham & Kokubun 1992). The instrumental calibration was repeated every 30 min. Absolute flux calibration was carried out daily, using the galactic source SgrB2 Main. The full dataset at 7 mm is presented in Table A.1.

2.2. Optical polarimetry at Pico dos Dias Observatory

Optical polarimetric observations of 3C 279 were carried out between 2009 and 2012 (MJD 54944 to MJD 56065), using the 0.6 m Boller & Chivens IAG/USP telescope and the imaging polarimeter IAGPOL (Magalhaes et al. 1996) working in linear polarization mode and with a standard *R*-band filter. The polarimeter consists of a rotatable, achromatic half-wave retarder, followed by a calcite Savart plate, such that it provides two images of each object in the field, with orthogonal polarizations between them, separated by 25.5 arcsec at the telescope focal plane. The simultaneous detection of the two beams allows observations under non-photometric conditions, and has the advantage that the sky polarization is practically canceled out. On photometric nights, the total flux density can be recovered by adding the two polarimetric components of a given image (Beaklini et al. 2017).

Two different CCDs were used throughout the monitoring program: a 1024 × 1024 pixel CCD of 24 microns per pixel and a 2048 × 2048 pixel CCD of 13.5 microns per pixel, both providing a field of view of about 10′ × 10′ (0.″67 pixel^{-1} and 0.″38 pixel^{-1}, respectively). On one typical night, between 1 and 5 polarimetric measurements were obtained, each consisting of

[2] Operated by Instituto Nacional de Pesquisas Espaciais (INPE/MCTIC).
[3] Operated by the Laboratório Nacional de Astrofísica (LNA/MCTIC).

eight images obtained from different wave plate positions separated by 22.5, consuming a mean total integration time of about 30 min, depending on sky quality.

The images were reduced with IRAF[4] usual routines to apply bias and flat-field corrections, while the polarimetric data were obtained using the PCCDPACK package (Pereyra 2000). The polarized standard stars used were HD 298383, HD 111579, and HD 155197 (Turnshek et al. 1990), while the lack of instrumental polarization was confirmed by observing the unpolarized stars HD 94851 (Turnshek et al. 1990) and WD 1620−391[5]. To compute calibrated flux densities throughout this work, a galactic extinction of $A_R = 0.076$ was considered (Schlegel et al. 1998). The full dataset of our polarimetric measurements is presented in Table A.2[6].

3. Results

In Fig. 1 we present our observations together with data at other wavelengths obtained from the literature. In the top panel (a) we show the 7 mm light curve obtained with the Itapetinga radiotelescope between 2009 and 2014 and the contemporaneous 7 mm flux density of the VLBI core, obtained from the VLBA-BU-BLAZAR Program[7]. A detailed description of that program can be found at Jorstad & Marscher (2016).

In the same Figure (b) we show the *R*-band light curve obtained from SMARTS[8] Optical/IR Observations of *Fermi* Blazars[9]. That program operates two small aperture telescopes located at Cerro Tololo Observatory to perform the photometric monitoring of a sample of blazars at *B*, *V*, *R*, *J*, and *K* bands (Bonning et al. 2012).

The light curve showing the source activity at γ rays in the same time span can be seen in the middle panel of Fig. 1c. To build the light curve, the *Fermi*/LAT data between 0.1 and 300 GeV were binned in intervals of 3 days in order to increase the S/N ratio (Hayashida et al. 2015). Finally, the variability in optical polarization degree and position angle obtained from our observations are shown in the two bottom panels (d and e).

Through the analysis of our single-dish 7 mm light curve we can see a systematic increase in the flux density along the years, and the superposition of several flares on shorter timescales. The strongest flare was observed in December 2011 (MJD 55917), when 3C 279 reached a maximum flux density of 48.8 ± 2.3 Jy. The minimum flux density of 10.7 ± 0.8 Jy was observed in 7 April 2010 (MJD 55293). The core emission obtained from VLBA images at the same frequency was generally smaller than that obtained in the single-dish observations, showing that a large part of the emission was produced in the parsec-scale jet, especially during the flares observed in 2011−2012.

At γ-ray wavelengths we see a large number of short timescale fluctuations at the beginning of the *Fermi*/LAT observations, and an isolated flare in 25 September 2010 (MJD 55465), followed by a small group of fast flares beginning in 15 April 2011 (MJD 55667), and lasting for approximately 70 days. This last group of flares occurred about five months before the beginning of the strong radio flare, reaching a flux of $(1.8 \pm 0.3) \times 10^{-6}$ ph s^{-1} cm^{-2}. At that moment, it was the highest flux detected at γ-ray wavelengths, but it was still an order of magnitude weaker than the flares detected several years later. A period of very low activity followed, which lasted until 2014 when a large number of high intensity γ-ray flares was detected (Hayashida et al. 2015; Paliya et al. 2015, 2016; Rani et al. 2017; Patiño-Álvarez et al. 2018); it was, unfortunately, at the end of our monitoring. Differently from the 7 mm single-dish light curve, we do not see any systematic increase in the γ-ray emission along the years.

At the *R* band, high activity occurred between 2011 and 2012, with several short-term flares superposed to a variable component on longer timescales. The first flare is almost coincident with the γ-ray flare of 15 April 2011 (MJD 55667). As can be seen from the light curves, the optical behavior is similar to that observed at radio wavelengths shifted by approximately five months, with the optical emission occurring first. In both light curves, the period of high activity seems to have the same duration, taking into account the sampling limitation. We show this behavior in detail in Fig. 2, where the optical light curve is shifted by 150 days and superposed to the radio data. This delay is confirmed by the discrete correlation function (DCF) analysis (Edelson & Krolik 1988), presented in Fig. 3. In the same figure, we also present the DCF between 7 mm and γ rays and *R* band and γ rays, where no correlation was found above the 3σ level.

In the polarimetric data, at least for 2011, we see an increase in PD and a rotation in PA simultaneously with the occurrence of the γ-ray flare of 15 April (MJD 55667). On longer timescales, we verify the existence of a gradual PA rotation in the $Q/I_p \times U/I_p$ plane, as shown in Fig. 4. Because of the sin 2PA and cos 2PA dependence of the Stokes parameters, a continuous and gradual rotation in PA will appear as consecutive quadrant changes in that plane. In 2010, we detected a slow and gradual rotation of about 100° over six months and, although there are gaps that prevent an unambiguous determination of the direction of rotation, this behavior was also observed by Aleksić et al. (2014) and by Kiehlmann et al. (2016).

The relation between PD and total *R* magnitude, obtained from our polarimetric observations, as described in Sect. 2.2, is shown in Fig. 5. We do not see any clear evidence of correlation, which was confirmed by a weak correlation coefficient of $r = 0.01$. Using data obtained between December 2009 and January 2010 (MJD 55173 to MJD 55206), Ikejiri et al. (2011) found $r = 0.41^{+0.21}_{-0.27}$, using magnitudes in the *V* band. However, based on observations during 2013 and 2014 where a sequence of strong optical flares was observed with counterparts in γ-rays, Rani et al. (2018) found evidence of an anti-correlation between optical polarization and flux density at *R* band, with $r = 0.76$.

4. Discussion

4.1. Multiwavelength flux density variability

The 7 mm (43 GHz) light curve of 3C 279 obtained with the Itapetinga radiotelescope, extending from the end of 2009 to March 2014 (MJD 55179 to MJD 56733), showed a very strong increase in activity at the end of 2011: the flux density doubled over a period of two months, and remained at this level during almost one year. Although this blazar was monitored by several observatories, no report of this behavior was found in the literature, probably because it corresponded to a period of very low optical and γ-ray activity.

[4] IRAF is distributed by the National Optical Astronomy Observatory, which is operated by the Association of Universities for Research in Astronomy, Inc., under cooperative agreement with the National Science Foundation.
[5] From the IAG/USP polarimetric group, available at: http://astroweb.iag.usp.br/~polarimetria/padroes/index.html
[6] In Table A.2 we present the PA values between 0° and 180°. In Fig. 1 we allowed values higher than 180° to avoid artificial jumps in PA.
[7] http://www.bu.edu/blazars/VLBAproject.html
[8] http://www.astro.yale.edu/smarts/
[9] http://www.astro.yale.edu/smarts/glast/home.php

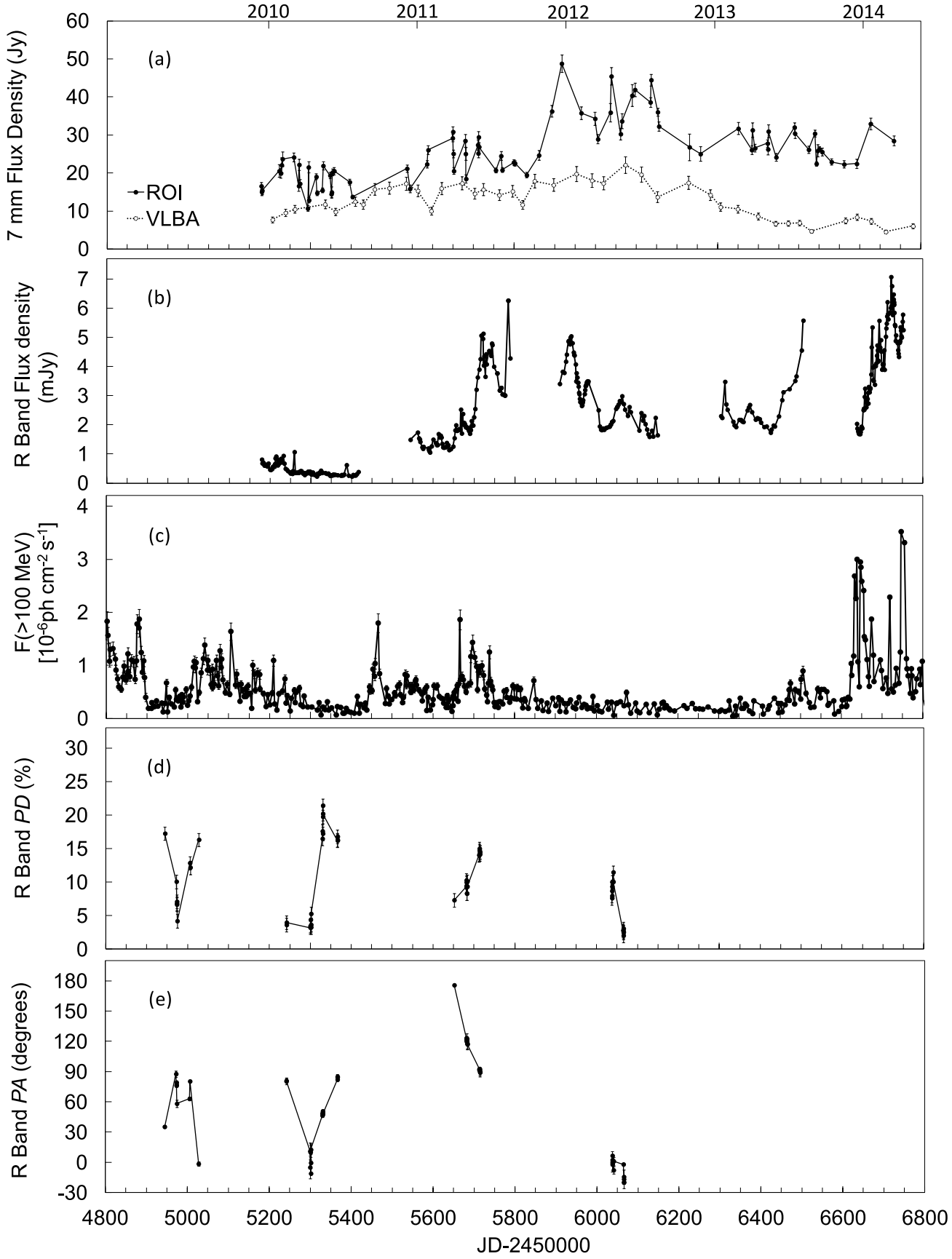

Fig. 1. Variability in 3C279 between 2009 and 2014. *(a)*: 7 mm single-dish light curve obtained in this work together with flux per beam of the peak obtained using VLBA data from the VLBA-BU BLAZAR monitoring project; *(b)*: *R*-band photometry from SMARTS; *(c)*: *Fermi*/LAT γ-ray light curve from Hayashida et al. (2015); *(d)*: *R*-band polarization degree (PD) and position angle (PA) obtained in this work.

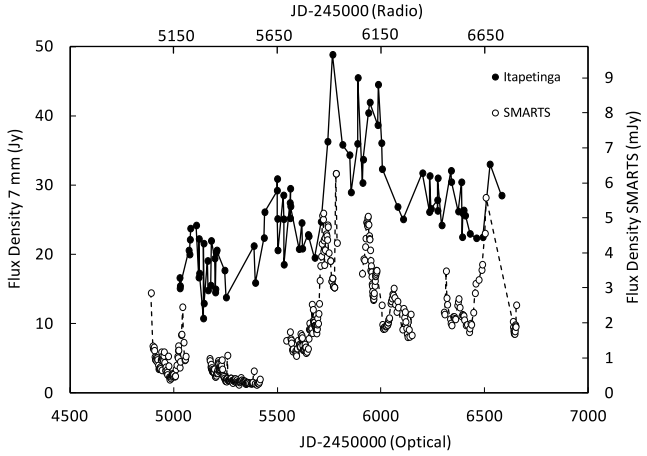

Fig. 2. Light curves of 3C 279 at radio (7 mm) and optical (*R*-band) wavelengths. The optical light curve scale is shifted by 150 days relative to radio.

During 2010 (MJD 54650 to MJD 55400), a good agreement was found between the Itapetinga light curve, the 43 GHz observations from Noto, and the 37 GHz observations from Metsähovi, as reported by Hayashida et al. (2012). Also, the Itapetinga 43 GHz observations between February and July 2011 (MJD 55600 and MJD 55740) also match very closely those at 37 GHz from Metsähovi Observatory, reported by Aleksić et al. (2014).

A correlation was found for the whole period between our 7 mm light curve and the *R*-band flux density from SMARTS, with a delay in radio of 170 ± 30 days relative to *R* band, as expected from a compact, optically thick source that becomes optically thin as it expands (Marscher & Gear 1985; Türler et al. 1999, 2000; Botti & Abraham 1988; Beaklini & Abraham 2014; Beaklini et al. 2017). A similar result was found by Chatterjee et al. (2008) for the period 1996−2007, using the *R* band and the 7 mm light curve of the core derived from VLBA images, obtaining a delay of 130^{+30}_{-45} days. The larger delay in the single-dish data, although within the uncertainty interval, can be explained if the emitting source left the core before reaching its maximum flux density. This is certainly the case of the strong flares at the end of 2011, detected in our 7 mm single-dish data, as can be seen in Fig. 1. Jorstad et al. (2017), in their analysis of the 43 GHz VLBA images for these epochs, found two components with intensities comparable to that of the core and very close to it. The position angles in the plane of the sky of these two components were very different from those of the other jet components.

The formation epoch of the superluminal components can be determined from their kinematic properties. From the work of Jorstad et al. (2017) we were able to follow the evolution of one of these strong components, with PA 155° ± 5° in the southeast direction, for which we found a velocity of 6.2*c* and a maximum flux density of around 9 Jy. It was formed around MJD 55430 (21 August 2010), coinciding with the beginning of a γ-ray flare that reached maximum flux density in MJD 55365. This component was also observed by Lu et al. (2013) at 230 GHz with the Event Horizon Telescope (EHT) on 1−2 April 2011, when it was at a distance of 0.13 mas from the core. From MJD ~ 55992 to MJD ~ 56075, a stationary component was seen in the VLBA images from Jorstad et al. (2017), at about a distance of 0.26 mas from the core, with position angle 175° and mean flux density of about 18 Jy. This component started moving at velocity 11*c* and PA rotating from −179° to −158°, while the flux density decreased from 20 Jy to 11 Jy in six months.

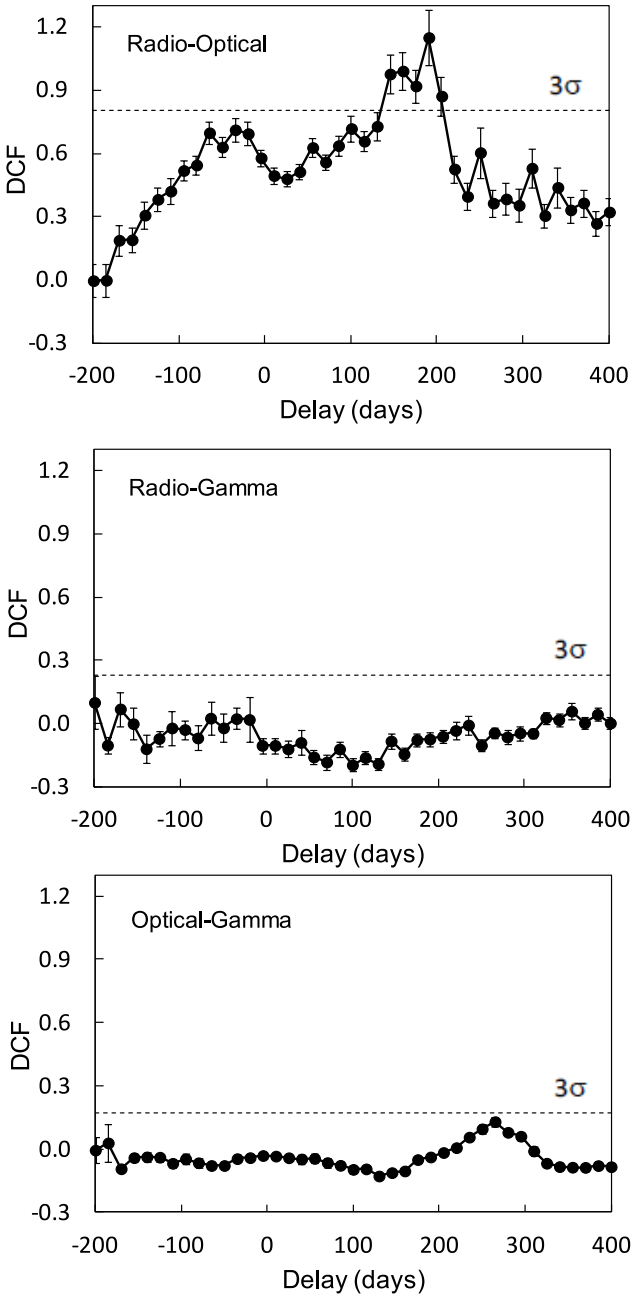

Fig. 3. DCF result between radio and optical (*top*), radio and γ rays (*middle*), γ rays and optical (*bottom*). The dashed line indicates the 3σ level. A significant peak at 170 ± 30 day can be seen in the DCF between the radio and optical light curves.

From the γ-ray light curve we can see, beginning in April 2011, a group of three flares (MJD 55667, 55697, and 55739) about 170 days before the beginning of the strong rise in the 7 mm light curve, which can be interpreted as the superposition of the radio counterparts of these γ-ray flares. The radio activity following this group of three flares was closely correlated with strong optical flares, taking into account the corresponding delay and lasting for about a year, but does not seem to have any strong γ-ray counterparts.

No correlation was found in the DCF between radio–γ-ray and *R*-band–γ-ray light curves, although this result does not mean that the emission is not produced in the same region. If the high energy emission is due to EC emission, it can be absorbed

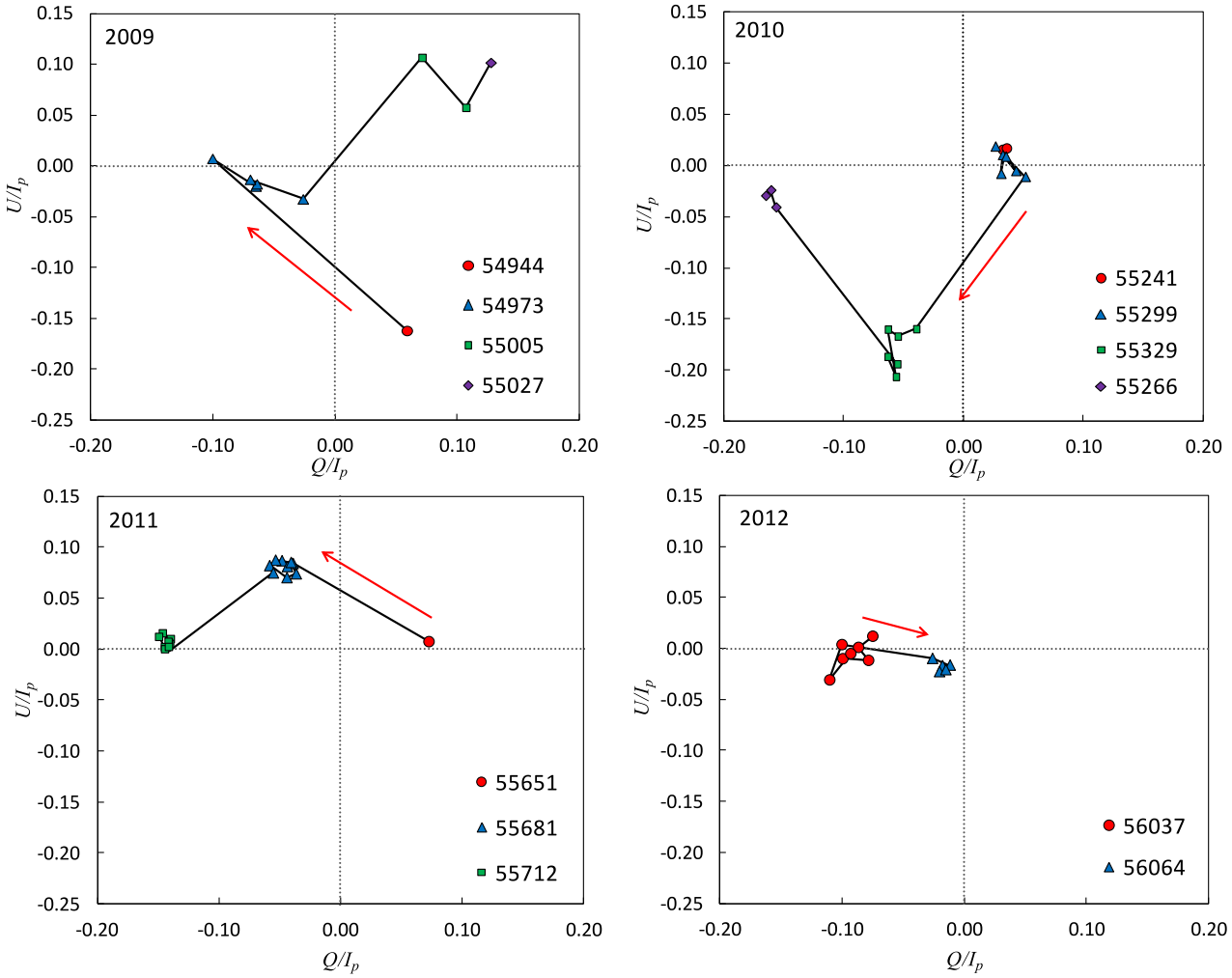

Fig. 4. Q x U Stokes plane normalized by I_p during the four years of our optical polarimetric monitoring. The arrows indicate the direction of increasing time.

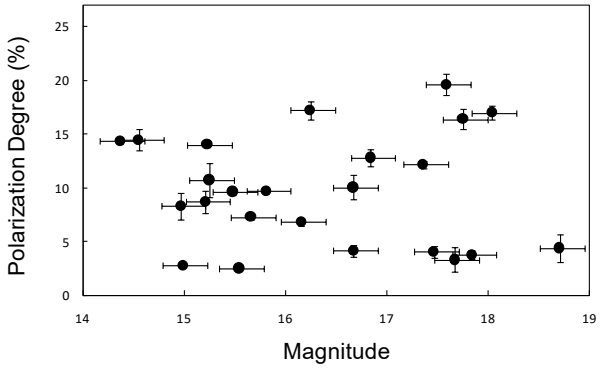

Fig. 5. PD vs. R-band magnitude recovered from our polarimetric images. No significant correlation was found based on the data.

by the photons of the broad line region (BLR) if emitted very close to the core (Böttcher & Els 2016), or it can be missing due to the lack of low energy photons in the beam direction.

4.2. Jet precession

The large variation (~80°) in the PA of the superluminal components formed during 2010−2012, together with the difference in their superluminal velocities, seems to support the idea of jet precession, as suggested by Abraham & Carrara (1998) and Qian (2011). The epoch in which the components are brighter and the variation in the position angles is larger and faster must correspond to the epoch when the angle between the jet and the line of sight is the smallest, as seems to have occurred between 2010 and 2012. Considering the precession model suggested by Abraham & Carrara (1998), with a period of 25 years, half the periodicity found by Webb et al. (1990), the epoch of closest approach would correspond to the year 2012. However Qian (2011) also found another large variation in the position angle of the superluminal components around 2006, which is compatible with a precession period of only 6 years, which is close to the period in the infrared found by Fan (1999). A longer and detailed analysis of the kinematics of the superluminal components would be necessary to confirm and fully understand jet precession.

4.3. Polarimetric variability

The existence of several components contributing to the total emission and their evolution along the jet can also present signatures on the polarimetric variability. A new polarized component can produce large changes in polarization parameters, but small changes are also possible depending on the values of the Stokes

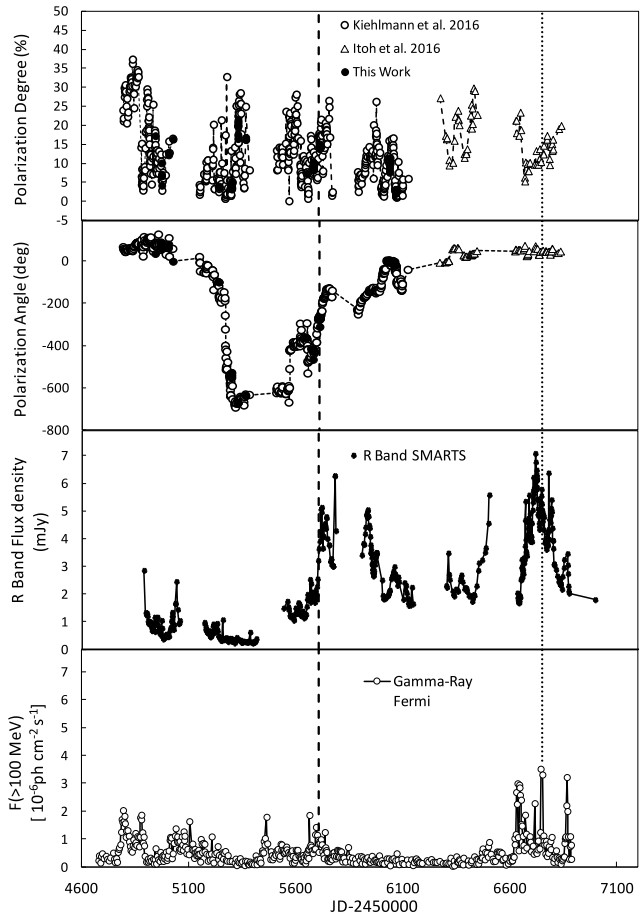

Fig. 6. *Top*: PA variability obtained by Kiehlmann et al. (2016) adding the data of this work. As a criterion to solve the 180° multiplicity we minimized the difference between successive data points. *Bottom*: *R*-band and γ-ray variability. The dashed line indicates the γ ray associated with a new jet component reported by Jorstad et al. (2017) that produced a PA rotation, while the dotted line indicates a new jet component seen in VLBI images (Rani et al. 2018) that did not produce changes in PA.

parameters of the jet and the new component (Beaklini et al. 2017). In 2011, we detected in our polarimetric data a gradual rotation of almost 200° in PA at the epoch of highest activity in the optical light curve. Around the same epoch, Aleksić et al. (2014) found a rotation of about 140°, while Kiehlmann et al. (2016) obtained 352°. These differences can be explained by gaps in the polarimetric monitoring, which can produce spurious rotation values (Kiehlmann et al. 2013, 2016; Beaklini et al. 2017, 2018).

In order to improve the data coverage of our analysis, we considered our data together with the PA measurements from Kiehlmann et al. (2016) and from Itoh et al. (2016). In the upper part of Fig. 6 we show the whole dataset that was used to solve the 180° multiplicity with the simplest assumption that between two consecutive observations PA changed by the lowest possible value, allowing both clockwise and counterclockwise rotation. This is an acceptable interpretation in the absence of large time lags between observations (Beaklini et al. 2018). We present the results in the second panel of Fig. 6, where it is possible to see that the PA rotated by almost 800° clockwise between MJD 54100 and 55300, without any clear counterpart in variability of the total flux density at *R* band and γ rays. After that large rotation, the PA rotated again by almost the same quantity and in a similar time interval, but counterclockwise, until it reached a level similar to that at the beginning of the monitoring.

This behavior of two directions of PA rotation was already detected in PKS 1510−089 (Beaklini et al. 2017) and OJ 287 (Cohen et al. 2018). In 3C 279, PA rotations were interpreted by Aleksić et al. (2014) as a consequence of the bending of the jet. We suggest that the rotations observed between 2010 and 2011 are the consequence of the ejection of a series of jet components during that epoch, as observed in the VLBI images reported by Jorstad et al. (2017) and identified by us in Sect. 4.1.

4.4. Polarimetric variability caused by the ejection of a new jet component

We followed the two component scenario described by Holmes et al. (1984) and applied it to describe the polarization variability due to the appearance of a new jet component. According to what was done in Beaklini et al. (2017) in the case of PKS 1510−089, we estimated the possible values of PD and PA of a new component that produced the observed change in PA.

To this end, we attributed a set of initial Stokes parameters for the whole jet, considering the emission of all the individual components. We computed the Stokes parameters after the emission of a new component using the following equations:

$$Q_{\rm final} = Q_{\rm jet} + Q_{\rm new}, \tag{1}$$

$$U_{\rm final} = U_{\rm jet} + U_{\rm new}, \tag{2}$$

$$I_{\rm p,final} = \sqrt{Q^2_{\rm final} + U^2_{\rm final}}, \tag{3}$$

where Q, U, and $I_{\rm p}$ are the Stokes parameters and the indexes *jet*, *final*, and *new* correspond to the quantities before and after the formation of a new component, and those of the new component, respectively. In principle, the polarimetric parameters U and Q of the new component can differ from the previous ones due to differences in magnetic field, particle densities, and/or geometry. We can write each parameter as a function of PA:

$$Q_{\rm jet} = I_{\rm p,jet} \cos 2\theta_{\rm jet}, \tag{4}$$

$$U_{\rm jet} = I_{\rm p,jet} \sin 2\theta_{\rm jet}, \tag{5}$$

where θ is the PA and the indexes remain the same. Solving the equation we obtain:

$$\cos 2\theta_{\rm final} = (I_{\rm p,jet} \cos 2\theta_{\rm jet} + I_{\rm p,new} \cos 2\theta_{\rm new})/I_{\rm p,final}, \tag{6}$$

$$\sin 2\theta_{\rm final} = (I_{\rm p,jet} \sin 2\theta_{\rm jet} + I_{\rm p,new} \sin 2\theta_{\rm new})/I_{\rm p,final}, \tag{7}$$

$$I^2_{\rm p,final} = I^2_{\rm p,jet} + I^2_{\rm p,new} + 2I_{\rm p,jet}I_{\rm p,new} \cos 2(\theta_{\rm new} - \theta_{\rm jet}). \tag{8}$$

Considering the epoch between 1 and 30 May 2011 (MJD 55693 and MJD 55711), the PA rotated from 117.°0 to 92.°4, while the PD increased from 9.3% to 14%. This variation could be attributed to a new component with a polarized optical flux of (0.028 ± 0.019) mJy and a PA of 138.°0 ± 2.°2. This new component appeared in the VLBI images presented by Jorstad et al. (2017) as discussed in Sect. 4.1. The ejection of a new component with such characteristics could change the direction of rotation, as shown by the dashed line in Fig. 6. On the other hand, as shown by Beaklini et al. (2017), a new component might not produce changes in PA, as is the case of NC2 (Rani et al. 2018) associated with the γ-ray flare in MJD 56756, indicated by the dotted line in Fig. 6.

5. Conclusions

We report five years of observations of 3C 279 at the 7 mm radio continuum and *R*-band polarimetry, obtained at the Itapetinga and Pico dos Dias observatories, respectively. We compared our monitoring with *R*-band total flux density obtained from the SMARTS program and γ-ray data from *Fermi*/LAT. We also used data from VLBA-BU-Blazar at 7 mm to compare our single-dish results with interferometric images, and we analyzed polarimetric variability together with the results reported by Kiehlmann et al. (2016). We can summarize our conclusions as follows:

- The 7 mm observations revealed a period of very high flux density starting at the end of 2011 and lasting for about a year.
- The 7 mm and *R*-band light curve from SMARTS showed very good correlation, with a lag of of 170 ± 30 days between radio and optical data.
- This delay also allowed us to associate a group of γ-ray flares observed in April 2011 with the rise, by a factor of two, in the 7 mm flux density at the end of 2011. However, no correlation was found between the 7 mm and γ-ray light curves for the whole period.
- During the occurrence of these γ-ray flares, polarimetric data showed an increase in PD and a large rotation in PA, which was interpreted as a consequence of the superposition of the polarimetric parameters of the jet and of a new component. The computed polarimetric parameters of this new component are (0.028 ± 0.019) mJy for the polarized flux and $138\overset{\circ}{.}0 \pm 2\overset{\circ}{.}2$ for PA.
- VLBA images showed, at the epoch of the 7 mm maximum, the appearance of two new components in the jet, ejected from the core with velocities of $6c$ and $11c$, with PAs in the plane of the sky very different from those of the other jet components.
- The differences in velocities and PAs of the different components are compatible with the jet precession models of Abraham & Carrara (1998) and Qian (2011), with a period of 25 years in the observer reference frame and maximum approach to the line of sight occurring in 2011.

Acknowledgements. We are grateful to the Brazilian research agencies FAPESP and CNPq for financial support (FAPESP Projects: 2008/11382-3 and 2014/07460-0). We thank INPE (Instituto Nacional de Pesquisas Espaciais) for the operation of ROI (Radio Observatório do Itapetinga). This study makes use of 43 GHz VLBA data from the VLBA-BU Blazar Monitoring Program (VLBA-BU-BLAZAR; http://www.bu.edu/blazars/VLBAproject.html), funded by NASA through the *Fermi* Guest Investigator Program. The VLBA is an instrument of the National Radio Astronomy Observatory. The National Radio Astronomy Observatory is a facility of the National Science Foundation operated by Associated Universities, Inc. This paper has made use of up-to-date SMARTS optical/near-infrared light curves that are available at www.astro.yale.edu/smarts/glast/home.php

References

Abdo, A. A., Ackermann, M., Ajello, M., et al. 2010, Nature, 463, 919
Abeysekara, A. U., Archambault, S., Archer, A., et al. 2015, ApJ, 815, L22
Abraham, Z., & Carrara, E. A. 1998, ApJ, 496, 172
Abraham, Z., & Kokubun, F. 1992, A&A, 257, 831
Albert, J., Aliu, E., Anderhub, H., et al. 2008, Science, 320, 1752
Aleksić, J., Antonelli, L. A., Antoranz, P., et al. 2011, A&A, 530, A4
Aleksić, J., Ansoldi, S., Antonelli, L. A., et al. 2014, A&A, 567, A41
Andruchow, I., Cellone, S. A., Romero, G. E., Dominici, T. P., & Abraham, Z. 2003, A&A, 409, 857
Atwood, W. B., Abdo, A. A., Ackermann, M., et al. 2009, ApJ, 697, 1071
Beaklini, P. P. B., & Abraham, Z. 2014, MNRAS, 437, 489
Beaklini, P. P. B., Dominici, T. P., & Abraham, Z. 2017, A&A, 606, A87
Beaklini, P., Dominici, T., & Abraham, Z. 2018, Galaxies, 6, 18
Bonning, E., Urry, C. M., Bailyn, C., et al. 2012, ApJ, 756, 13
Böttcher, M. 2007, Ap&SS, 309, 95
Böttcher, M. 2010, in Proceedings of the Workshop "Fermi meets Jansky: AGN in Gamma Rays", eds. T. Savolainen, E. Ros, R. W. Porcas, & J. A. Zensus (Bonn, Germany: Max-Plank-Institut für Radioastronomy), 41
Böttcher, M., & Els, M. 2016, ApJ, 821, 102
Böttcher, M., Reimer, A., & Marscher, A. P. 2009, ApJ, 703, 1168
Böttcher, M., Reimer, A., Sweeney, K., & Prakashi, A. 2013, ApJ, 768, 54
Botti, L. C. L., & Abraham, Z. 1988, AJ, 96, 465
Carrara, E. A., Abraham, Z., Unwin, S. C., & Zensus, J. A. 1993, A&A, 279, 83
Cerruti, M., Lenain, J. P., Prokoph, H., & H. E. S. S. Collaboration 2017, 35th Int. Cosmic Ray Conf., Bexco, Busan, Korea, Proc. Science, 301, 627
Chatterjee, R., Jorstad, S. G., Marscher, A. P., et al. 2008, ApJ, 689, 79
Cohen, M. H., Cannon, W., Purcell, G. H., et al. 1971, ApJ, 170, 207
Cohen, M. H., Aller, H. D., Aller, M. F., et al. 2018, ApJ, 862, 1
Collmar, W., Böttcher, M., Krichbaum, T. P., et al. 2010, A&A, 522, A66
Edelson, R., & Krolik, J. 1988, ApJ, 333, 646
Fan, J. H. 1999, MNRAS, 308, 1032
Ghisellini, G., Celotti, A., Fossati, G., Maraschi, L., & Comastri, A. 1998, MNRAS, 301, 451
Hartman, R. C., Bertsch, D. L., Fichtel, C. E., et al. 1992, ApJ, 385, L1
Hartman, R. C., Böttcher, M., Aldering, G., et al. 2001a, ApJ, 553, 683
Hatman, R. C., Villalta, M., Balonek, T. J., et al. 2001b, ApJ, 558, 583
Hayashida, M., Madejski, G. M., Nalewajko, K., et al. 2012, ApJ, 754, 114
Hayashida, M., Nalewajko, K., Madejski, G. M., et al. 2015, ApJ, 807, 79
Holmes, P. A., Brand, P. W. J. L., Impey, C. D., et al. 1984, MNRAS, 211, 497
Ikejiri, Y., Uemura, M., Sasada, M., et al. 2011, PASJ, 63, 639
Itoh, R., Nalewajko, K., Fukazawa, Y., et al. 2016, ApJ, 833, 77
Jermak, H., Steele, I. A., Lindfors, E., et al. 2016, MNRAS, 462, 4267
Jorstad, S., & Marscher, A. 2016, Galaxies, 4, 47
Jorstad, S. G., Marscher, A., Morozova, D. A., Troitsky, I. S., & Agudo, I. 2017, ApJ, 846, 98
Kiehlmann, S., Savolainen, T., Jorstad, S. G., et al. 2013, Eur. Phys. J. Web Conf., 61, 06003
Kiehlmann, S., Savolainen, T., Jorstad, S. G., et al. 2016, A&A, 590, A10
Kinman, T. D. 1967, ApJ, 148, L53
Larionov, V. M., Jorstad, S. G., Marscher, A. P., et al. 2008, A&A, 492, 389
Magalhaes, A. M., Rodrigues, C. V., Margoniner, V. E., Pereyra, A., & Heathcote, S. 1996, Polarimetry of the Interstellar Medium, 97, 118
Mannheim, K. 1993, A&A, 269, 67
Liu, R.-Y., Wang, K., Xue, R., et al. 2019, Phys. Rev. D, 99, 63008
Lu, R.-S., Fish, V. L., Akiyama, K., Doeleman, S. S., & Algaba, J. C. 2013, ApJ, 772, 13
Maraschi, L., Grandi, P., Urry, C. M., et al. 1994, ApJ, 435, 191
Marscher, A. P., & Gear, W. K. 1985, ApJ, 298, 114
Marscher, A. P., Jorstad, S. G., Larionov, V. M., et al. 2010, ApJ, 710, L126
Max-Moerbeck, W., Hovatta, T., Richards, J. L., et al. 2014, MNRAS, 445, 428
Mead, A. R. G., Ballard, K. R., Brand, P. W. J. L., et al. 1990, A&AS, 83, 183
Mirzoyan, R. 2014, ATel, 6349
Mirzoyan, R. 2017, ATel, 11061
Paliya, V. S., Sahayanathan, S., & Stalin, C. S. 2015, ApJ, 803, 15
Paliya, V. S., Diltz, C., Böttcher, M., Stalin, C. S., & Buckley, D. 2016, ApJ, 817, 61
Patiño-Álvarez, V. M., Fernandes, S., Chavushyan, V., et al. 2018, MNRAS, 479, 2037
Pereyra, A. 2000, PhD Thesis, University of São Paulo
Pian, E., Urry, C. M., Maraschi, L., et al. 1999, ApJ, 521, 112
Qian, S.-J. 2011, Res. Astron. Astrophys., 11, 43
Rani, B., Krichbaum, T. P., Lee, S.-S., et al. 2017, MNRAS, 464, 418
Rani, B., Jorstad, S. G., Marscher, A., Agudo, I., Sokolovsky, K. V., et al. 2018, ApJ, 858, 80
Schlegel, D. J., Finkbeiner, D. P., & Davis, M. 1998, ApJ, 500, 525
Stevens, J. A., Robson, E. I., Gear, W. K., et al. 1998, ApJ, 502, 182
Türler, M., Paltani, S., Courvoisier, T. J.-L., et al. 1999, A&AS, 134, 89
Türler, M., Corvoisier, T. J.-L., & Paltani, S. 2000, A&A, 361, 850
Turnshek, D. A., Bohlin, R. C., Williamson, II., R. L., et al. 1990, AJ, 99, 1243
Webb, J. R., Carini, M. T., Clements, S., et al. 1990, AJ, 100, 1452
Wehrle, A. E., Pian, E., Urry, C. M., et al. 1998, ApJ, 497, 178
Whitney, A. R., Shapiro, I. I., Rogers, A. E. E., et al. 1971, Science, 173, 225

Appendix A: Tables

Table A.1. Radio flux density obtained in this work.

Day	JD-2400000	Flux density (Jy)	Error	Day	JD-2400000	Flux density (Jy)	Error
2009-12-14	55179	16.59	0.99	2011-08-26	55799	22.81	0.78
2009-12-15	55180	15.07	0.92	2011-08-29	55802	22.60	0.72
2009-12-16	55181	15.42	1.01	2011-09-27	55831	19.48	0.71
2010-01-27	55223	20.56	1.64	2011-10-27	55861	24.69	1.24
2010-01-31	55227	19.97	1.27	2011-11-28	55893	36.26	1.55
2010-02-02	55229	22.11	1.97	2011-12-22	55917	48.82	2.27
2010-02-04	55231	23.72	1.92	2012-02-08	55965	35.81	1.68
2010-03-04	55259	24.17	1.11	2012-03-13	55999	34.33	1.77
2010-03-16	55271	16.64	1.41	2012-03-20	56006	28.93	1.22
2010-03-17	55272	22.22	1.42	2012-04-20	56037	35.96	2.42
2010-03-19	55274	17.23	1.03	2012-04-22	56039	45.48	2.29
2010-04-07	55293	10.73	0.77	2012-05-15	56062	30.30	1.58
2010-04-09	55295	21.55	1.43	2012-05-18	56065	33.67	1.97
2010-04-10	55296	12.89	0.67	2012-06-12	56090	40.41	2.85
2010-04-28	55314	19.05	0.79	2012-06-19	56097	41.93	1.77
2010-04-30	55316	14.78	0.64	2012-07-27	56135	38.64	1.27
2010-05-13	55329	15.49	0.69	2012-07-29	56137	44.50	1.51
2010-05-15	55331	21.94	1.12	2012-08-14	56153	36.05	1.00
2010-06-01	55348	19.39	0.89	2012-08-18	56156	32.30	1.19
2010-06-04	55351	14.48	0.94	2012-10-31	56231	26.84	3.52
2010-06-05	55352	14.96	1.45	2012-11-27	56258	25.05	1.94
2010-06-07	55354	20.25	0.92	2013-02-28	56351	31.72	1.59
2010-06-11	55358	20.57	0.94	2013-04-02	56384	26.10	1.11
2010-07-19	55396	17.66	0.79	2013-04-04	56386	31.31	1.90
2010-07-26	55403	13.76	0.44	2013-04-10	56392	26.56	1.03
2010-12-07	55537	21.20	0.98	2013-05-11	56423	27.82	0.93
2010-12-14	55544	15.86	1.05	2013-05-12	56424	26.27	1.45
2011-01-25	55586	22.35	0.98	2013-05-13	56425	30.98	1.69
2011-01-28	55589	26.09	1.18	2013-06-01	56444	24.17	0.96
2011-03-29	55649	29.20	0.95	2013-07-16	56489	32.06	1.19
2011-03-30	55650	30.87	1.39	2013-07-17	56490	30.43	1.27
2011-03-31	55651	25.11	1.01	2013-08-20	56524	26.18	0.92
2011-04-01	55652	20.57	0.92	2013-09-04	56539	30.41	0.89
2011-04-29	55680	28.51	1.64	2013-09-08	56543	22.47	0.61
2011-04-30	55681	25.07	1.63	2013-09-11	56546	25.87	1.63
2011-05-01	55682	18.50	1.12	2013-09-15	56550	26.34	0.68
2011-05-30	55711	27.42	1.31	2013-09-22	56557	25.58	1.07
2011-05-31	55712	25.20	1.2	2013-10-15	56580	22.96	0.83
2011-06-01	55713	29.48	1.51	2013-11-15	56611	22.32	0.91
2011-06-02	55714	26.91	1.13	2013-12-16	56642	22.46	1.20
2011-07-13	55755	20.75	0.68	2014-01-19	56676	32.99	1.50
2011-07-26	55768	24.53	1.18	2014-03-17	56733	28.48	1.27
2011-07-29	55771	20.81	0.65				

Table A.2. *R*-flux density and polarization of 3C 279 obtained in this work.

Date	JD −2450000	Q/I	U/I	Total flux mJy	Error mJy	Polarized flux mJy	Error mJy	*PD* %	Error %	*PA* degrees	Error degrees
2009-04-22	4944.56	0.059	−0.162	0.94	0.28	0.16	0.04	17.2	0.8	35.2	1.4
2009-05-20	4972.51	−0.100	0.007	0.63	0.19	0.06	0.03	10.1	1.1	87.6	3.2
2009-05-21	4973.47	−0.065	−0.020	1.01	0.30	0.07	0.02	6.8	0.2	76.0	0.9
2009-05-21	4973.53	−0.064	−0.018	1.01	0.30	0.07	0.02	6.6	0.3	76.8	1.2
2009-05-21	4973.59	−0.070	−0.013	1.01	0.30	0.07	0.02	7.1	0.5	79.1	2.0
2009-05-22	4974.50	−0.026	−0.032	0.63	0.19	0.03	0.01	4.2	0.5	58.1	3.7
2009-06-22	5005.45	0.071	0.107	0.54	0.16	0.07	0.03	12.8	0.8	63.0	1.8
2009-06-23	5006.44	0.107	0.058	–	–	–	–	12.2	0.3	80.3	0.8
2009-07-14	5027.43	0.127	0.102	0.33	0.10	0.05	0.04	16.3	1.1	178.4	1.9
2010-02-13	5241.78	0.032	0.016	0.21	0.06	0.01	0.01	3.6	0.4	80.5	3.5
2010-02-13	5241.81	0.036	0.017	0.21	0.06	0.01	0.01	4.0	0.3	80.7	2.3
2010-04-12	5299.60	0.031	−0.008	0.25	0.08	0.01	0.01	3.2	1.0	190.9	8.6
2010-04-12	5299.64	0.032	0.011	0.25	0.08	0.01	0.01	3.4	1.3	174.9	11.2
2010-04-13	5300.62	0.044	−0.005	0.10	0.03	0.00	0.01	4.4	1.3	189.8	8.4
2010-04-14	5301.57	0.026	0.019	0.30	0.09	0.01	0.01	3.2	0.1	168.8	0.9
2010-04-14	5301.59	0.035	0.009	0.30	0.09	0.01	0.01	3.6	0.7	179.4	5.4
2010-04-14	5301.62	0.051	−0.011	0.30	0.09	0.02	0.01	5.3	0.9	12.5	4.7
2010-05-12	5329.52	−0.040	−0.160	0.18	0.05	0.03	0.03	16.5	0.9	46.3	1.5
2010-05-12	5329.62	−0.055	−0.167	0.18	0.05	0.03	0.04	17.6	0.4	48.4	0.6
2010-05-13	5330.52	−0.063	−0.160	0.27	0.08	0.05	0.04	17.2	0.9	50.7	1.4
2010-05-13	5330.54	−0.056	−0.206	0.27	0.08	0.06	0.05	21.4	1.3	47.6	1.7
2010-05-13	5330.59	−0.063	−0.187	0.27	0.08	0.05	0.04	19.7	0.8	49.3	1.1
2010-05-13	5330.62	−0.055	−0.194	0.27	0.08	0.05	0.04	20.2	1.0	47.9	1.4
2010-06-18	5366.44	−0.157	−0.041	0.23	0.07	0.04	0.03	16.2	0.8	82.0	1.4
2010-06-18	5366.47	−0.161	−0.024	0.23	0.07	0.04	0.04	16.3	1.2	85.0	2.2
2010-06-18	5366.51	−0.165	−0.029	0.23	0.07	0.04	0.04	16.8	0.9	84.2	1.5
2011-03-30	5651.63	0.073	0.008	1.61	0.48	0.12	0.02	7.3	0.2	175.7	0.9
2011-04-29	5681.47	−0.039	0.084	1.89	0.57	0.18	0.02	9.3	0.0	123.3	0.0
2011-04-29	5681.50	−0.048	0.087	1.89	0.57	0.19	0.02	9.9	0.2	121.2	0.6
2011-04-29	5681.53	−0.053	0.088	1.89	0.57	0.19	0.04	10.3	0.8	120.0	2.3
2011-04-29	5681.56	−0.044	0.081	1.89	0.57	0.17	0.02	9.2	0.2	121.6	0.6
2011-04-29	5681.58	−0.041	0.085	1.89	0.57	0.18	0.02	9.5	0.3	123.0	0.9
2011-04-30	5682.53	−0.037	0.074	3.03	0.91	0.25	0.07	8.3	1.7	122.2	5.9
2011-04-30	5682.57	−0.044	0.070	3.03	0.91	0.25	0.05	8.3	1.2	119.3	4.1
2011-05-01	5683.57	−0.058	0.082	1.39	0.42	0.14	0.02	10.1	0.3	117.5	1.0
2011-05-01	5683.60	−0.055	0.075	1.39	0.42	0.13	0.02	9.3	0.1	117.0	0.4
2011-05-30	5712.47	−0.140	0.010	2.39	0.72	0.33	0.04	14.0	0.3	92.4	0.7
2011-05-30	5712.50	−0.140	0.005	2.39	0.72	0.34	0.03	14.0	0.2	91.5	0.4
2011-05-31	5713.43	−0.142	0.008	4.46	1.34	0.63	0.13	14.2	2.3	91.1	4.6
2011-05-31	5713.48	−0.146	0.016	4.46	1.34	0.66	0.03	14.7	0.1	92.7	0.2
2011-05-31	5713.54	−0.149	0.012	4.46	1.34	0.67	0.04	15.0	0.1	92.0	0.2
2011-06-01	5714.43	−0.145	0.002	5.28	1.58	0.76	0.05	14.5	0.3	89.5	0.7
2011-06-01	5714.46	−0.144	0.000	5.28	1.58	0.76	0.03	14.4	0.1	89.1	0.1
2011-06-01	5714.49	−0.141	0.002	5.28	1.58	0.75	0.05	14.1	0.3	89.5	0.7
2012-04-19	6037.50	−0.075	0.012	2.42	0.73	0.18	0.08	7.6	2.7	186.5	10.0
2012-04-19	6037.55	−0.087	0.001	2.42	0.73	0.21	0.04	8.7	1.0	182.3	3.4
2012-04-19	6037.56	−0.078	−0.012	2.42	0.73	0.19	0.04	7.9	1.1	177.7	4.1
2012-04-19	6037.60	−0.100	−0.010	2.42	0.73	0.24	0.03	10.0	0.3	179.1	0.8
2012-04-19	6037.63	−0.093	−0.005	2.42	0.73	0.23	0.02	9.3	0.2	0.4	0.7
2012-04-22	6040.48	−0.110	−0.031	2.34	0.70	0.27	0.02	11.5	0.0	172.1	0.1
2012-04-22	6040.53	−0.100	0.004	2.34	0.70	0.23	0.09	10.0	3.2	181.0	9.1
2012-05-16	6064.46	−0.026	−0.010	2.98	0.89	0.08	0.01	2.8	0.2	177.9	1.6
2012-05-17	6065.46	−0.012	−0.016	1.79	0.54	0.04	0.01	2.0	0.2	159.9	2.3
2012-05-17	6065.49	−0.018	−0.017	1.79	0.54	0.04	0.01	2.5	0.2	165.5	2.4
2012-05-17	6065.52	−0.020	−0.023	1.79	0.54	0.05	0.01	3.1	0.1	163.1	1.0
2012-05-17	6065.55	−0.015	−0.021	1.79	0.54	0.05	0.01	2.6	0.1	160.2	1.2

Notes. PA values have a multiplicity of $+n180°$.